Modelling Optimisation of Distributed PV-Battery Charge and Discharge Modes Using Systems for Improved Sustainable Energy Management

Manuscript received October 23, 2025; revised January 29, 2026

Syamsyarief Baqaruzi*
Department of Electrical Engineering
Institut Teknologi Sumatera
South Lampung, Indonesia
syamsyarief.baqaruzi@el.itera.ac.id

Amrina Mustaqim
Department of Physics Engineering
Institut Teknologi Sumatera
South Lampung, Indonesia
amrina.mustaqim@tf.itera.ac.id

Ali Muhtar
Department of Electrical Engineering
Institut Teknologi Sumatera
South Lampung, Indonesia
ali.muhtar@el.itera.ac.id

Muhammad Rizky Hikmatullah
Department of Telecommunication Engineering
Institut Teknologi Sumatera
South Lampung, Indonesia
muhammad.hikmatullah@tt.itera.ac.id

Rahmat Fadhilah
Department of Mining Engineering
Institut Teknologi Sumatera
South Lampung, Indonesia
rahmat.fadhilah@ta.itera.ac.id

Andika Munandar
Department of Envinronment Engineering
Institut Teknologi Sumatera
South Lampung, Indonesia
andika.munandar@tl.itera.ac.id

Edo Kharisma Army
Department of Mining Engineering
Institut Teknologi Sumatera
South Lampung, Indonesia
edo.army@ta.itera.ac.id

Setiadi Wira Buana
Department of Energy System Engineering
Institut Teknologi Sumatera
South Lampung, Indonesia
setiadi.wira@tse.itera.ac.id

Rizqi Wahyudi
Department of Industrial Engineering
Institut Teknologi Sumatera
South Lampung, Indonesia
rizky.wahyudi@ti.itera.ac.id

Muhammad Rifqi Dwi S
Department of Oil and Gas Engineering
Institut Teknologi Sumatera
South Lampung, Indonesia
muhammad.s@rmg.itera.ac.id

***Abstract*— This study examines the simulation of charge and discharge modes of lithium-ion batteries in a distributed photovoltaic system using MATLAB/ Simulink modeling. The objective is to analyze the integration of solar panels with battery-based energy storage systems to optimize performance and efficiency. The methodology involves mathematical modeling of photovoltaic cells based on p-n junctions, with key parameters such as temperature (15–30°C) and irradiance (1000 W/m²), along with the design of a Solar Charge Controller (SCC) to regulate energy flow. Simulations were conducted on four 150 W photovoltaic panels under varying environmental conditions, integrated with parallel-connected 12 V 250 Ah batteries. Results show a system efficiency of 87% at 25°C and 1000 W/m² irradiance, with panel output voltages aligning with mathematical equations (0.15 A error). Discharge mode analysis, accounting for system losses (inverter 5%, SCC 3%, wiring 2%), confirms the battery can supply a 5 Ω load for approximately 2.00 hours at 45% State of Charge (SOC), representing a 9.5% reduction from the ideal calculation. Simulations also compare SCC performance using DC and photovoltaic sources, demonstrating consistency in energy flow regulation. Validation results indicate the Simulink model's accuracy in representing real-world characteristics, though Matlab code simulations exhibit higher precision. The study highlights the importance of SCC control and SOC management to enhance battery lifespan and stability in renewable hybrid energy systems. Implications include potential applications**

Keywords*— *Charge-Discharge, Lithium-Ion Battery, Photovoltaic, Renewable Energy, Simulink

I. INTRODUCTION

Renewable energy sources (RES), including solar, wind, hydro, geothermal, and biomass, offer abundant and geographically distributed potential [1], [2]. However, their integration into global electricity systems faces significant technical and economic challenges. Conventional power generation systems [3] exhibit declining operational efficiency and rising costs when retrofitted with advanced monitoring and control infrastructure. Consequently, hybrid renewable energy systems (HRES) have gained considerable research attention. Recent studies [4], [5], [6] have developed mathematical models of photovoltaic panels, battery storage, and power converters, validated through Matlab/Simulink simulations that closely replicate real-world system behavior.

Rechargeable batteries are fundamental electrochemical devices, transforming electrical energy into chemical energy during charging and vice versa during discharge [7]. These devices play a significant role in the future technological landscape, particularly as potential energy storage elements in various green technology applications [8], [9]. Batteries are an indispensable component in crucial systems such as

 EISSN: 2961-872X ● PISSN: 2961-8924 ● DOI: 10.56741/IISTR.esl.001508

electric vehicles (EVs), hybrid electric vehicles (HEVs), solar energy systems, and smart grid systems [10], [11]. Lithium-ion batteries are widely preferred due to their rechargeability and superior energy-to-power ratio compared to other lead-acid and nickel-metal hydride batteries [12], [13]. In designing systems involving batteries, a thorough understanding of their behavior is essential for predicting performance [14] and optimizing energy dissipation [15]. Therefore, information related to the charging and discharging processes of lithium-ion batteries is a crucial factor in circuit design to achieve high performance and power efficiency. Various parameters related to battery behavior, including State of Charge (SOC), play a crucial role. Battery SOC information provides an indication of charge/discharge control, making accurate SOC determination crucial in any battery-based storage system [16], [17], [18].

The percentage of remaining energy capacity in a battery relative to its maximum capacity serves as an indicator of available power. One common method for estimating SOC is Coulomb Counting (CC), which calculates the charge by integrating the current entering/leaving the battery over time. While simple and easy to implement, this method is susceptible to accumulated errors due to sensor inaccuracies, charging efficiency, or external factors such as temperature [17], [19]. Therefore, it is often combined with voltage calibration or advanced models to improve accuracy in battery management systems. Technological innovation focused on the development of renewable energy is crucial for creating a more reliable, efficient, and environmentally friendly energy system [20]. This study aims to examine the implementation of battery development technology that has enabled the modeling of photovoltaic systems integrated with lithium-ion batteries for charge-discharge simulations using MATLAB [21].

Critical simulations in Simulink and MATLAB code were performed to test various architectures' internal behavior. Finally, these simulations were translated into a physical system, testing each component and behavior [22]. The main result was that the Simulink simulations had lower precision than those performed in Matlab code, while the results obtained were nearly identical to those found in real systems [23]. An electrical equivalent circuit model of a lithium-ion cell demonstrated the model's suitability for effective monitoring of SOC and battery health [24].

Furthermore, a Simulink model based on the equivalent circuit was developed. Recent advancements in battery technology have sustained the demand for electricity generation, while remote regions continue to face restricted access due to their distance from power generation facilities [25]. The ongoing dependence on traditional energy sources, especially those derived from fossil fuel burning, has multifaceted ramifications that include environmental, economic, and geopolitical dimensions [26], [27], [28], [29]. The finite nature of fossil reserves and their environmental externalities necessitate renewable energy adoption. Unlike fossil fuels, renewable energy sources (RES) are geographically widespread and essentially inexhaustible [30], [31], [32].

However, conventional power generation systems face persistent challenges in operational efficiency and long-term performance when integrated with complex embedded components [33]. An electrical equivalent circuit model of a lithium-ion cell illustrated the model's efficacy for proficient monitoring of state of charge and battery health. Additionally, a Simulink model based on the comparable circuit was created.

While previous studies have explored various aspects of PV-battery systems, this work uniquely focuses on distributed small-scale systems (600 W) with detailed Solar Charge Controller (SCC) logic and comparative analysis between Simulink and Matlab code implementations. This study aims to examine the implementation of battery development technology that has enabled the modeling of photovoltaic systems integrated with lithium-ion batteries for charge-discharge simulations using MATLAB/Simulink. The main contributions are:

1. detailed modeling of a PI-controlled SCC for distributed PV battery systems,
2. comprehensive loss analysis in system efficiency calculations, and
3. quantitative comparison between Simulink and matlab implementations.

II. Research Methods

Photovoltaic energy conversion is fundamentally based on p–n junction operation; however, detailed semiconductor physics is beyond the scope of this study. Accordingly, the photovoltaic module is modeled using a classical single-diode equivalent circuit, which offers a suitable trade-off between modeling accuracy and computational efficiency for system-level simulations. The analyzed off-grid system has a total rated capacity of 600 W and integrates a DC–DC buck–boost converter acting as a Solar Charge Controller (SCC) to perform Maximum Power Point Tracking (MPPT) and regulate power flow between the photovoltaic array and the lithium-ion battery, as illustrated in Fig. 1.

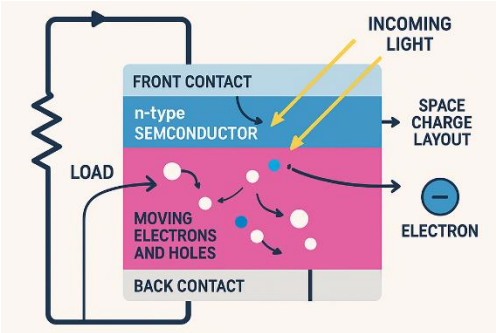


Fig. 1. Photovoltaic structure based on p-n junction

The energy conversion process commences when a photon of light impacts the photovoltaic surface. Adequate photon energy ionises semiconductor atoms, generating electron-hole (e-h) pairs. The electric field in the Space Charge Layer (SCL) separates these pairs: electrons are directed towards the n-type layer, while holes move towards the p-type layer. This charge separation establishes a potential difference between the front contact (negative terminal) and the back contact (positive terminal). When both terminals are linked to an external load, electrons traverse from the n-type layer to the p-type layer via the external circuit, producing direct current.

The photovoltaic system is modeled using the single-diode equivalent circuit, which is widely accepted for its balance between accuracy and simplicity. The model consists of a current source, a diode, series resistance (Rs), and shunt resistance (Rsh). The output current is given by Equation (1)

$$I = I_{ph} - I_0 \left[\exp\left(\frac{V + I R_s}{n V_{th}}\right) - 1 \right] - \frac{V + IR_s}{R_{sh}} \quad (1)$$

$$I_{ph} = [I_{sc} + K_i(T - T_n)]\frac{G}{G_n} \quad (2)$$

$$I_0 = I_{rs}\left(\frac{T}{T_n}\right)^3 \exp\left[\frac{qE_g}{nk}\left(\frac{1}{T_n} - \frac{1}{T}\right)\right] \quad (3)$$

The photocurrent depends on irradiance and temperature using equation (2) where $V_{th} = kT/q$ is the thermal voltage, I_{ph} is the photocurrent, I_0 is the diode saturation current, n is the ideality factor, R_s is the series resistance, and R_{sh} is the shunt resistance. where I_{sc} is the short-circuit current at nominal conditions, K_i is the temperature coefficient, T is the operating temperature, $T_n = 298\,k$ is the nominal temperature, G is the irradiance, and $G_n = 1000\,Wm^{-2}$ is the nominal irradiance.

The diode saturation current varies with temperature using Equation (3), where I_{rs} is the reverse saturation current at nominal conditions and E_g is the bandgap energy of the semiconductor. The system configuration of four 150-watt panels (total 600 watts) was selected to represent typical residential installations in Indonesia, providing sufficient capacity for basic household loads while maintaining scalability for distributed applications.

Photovoltaic efficiency is fundamentally governed by the material's optical absorption capacity and the suppression of electron-hole recombination within the space charge region. Consequently, optimizing the interface layer design and doping profiles is critical for maximizing charge carrier generation and collection. Furthermore, computational modeling of p-n junction characteristics using platforms such as MATLAB is frequently employed to predict system performance under dynamic environmental conditions, including variations in irradiance and temperature

$$I_{\text{ph}} = [I_{\text{sc}} + K_i(T - 298)] \times \frac{I_r}{1000} \quad (4)$$

$$I = \frac{V + I \cdot R_s}{R_{\text{sh}}} \quad (5)$$

$$I_0 = I_{\text{rs}} \cdot \left(\frac{T}{T_n}\right)^3 \cdot \exp\left(\frac{q \cdot E_g}{n \cdot k}\left(\frac{1}{T_n} - \frac{1}{T}\right)\right) \quad (6)$$

$$I = I_{\text{ph}} - I_0 \cdot \left(\exp\left(\frac{q \cdot (V + I \cdot R_s)}{n \cdot k \cdot N_s \cdot T}\right) - 1\right) - \frac{V + I \cdot R_s}{R_{\text{sh}}} \quad (7)$$

This study presents calculations from Equation (4) to Equation (7) to validate the simulation findings against the actual outcomes in the mathematical model computations. A parameter table is presented to facilitate the study of the acquired simulation results.

Photovoltaic design in Simulink Matlab that receives input in the form of temperature (T) and Irradiance (Ir) parameters. From the input given, it produces an output in the form of DC voltage that can be used for daily needs, or can be stored in a battery using a Solar Charge Controller (SCC).

TABLE I. PARAMETERS FOR MATHEMATICAL MODELLING

Abbr.	Description	Value	Unit
Iph	Photo-current	8.21	A
Isc	Short Circuit Current	8.21	A
Ki	Short-circuit current temperature coefficient	0.0032	A/K
T	Operating Temperature	298 (25°C)	K
Tn	Nominal Temperature	298	K
G	Irradiance	1000	W/m²
q	Electron charge	1.602×10^{-19}	C
Voc	Open Circuit Voltage	32.9	V
n	Ideality factor of the diode	1.3	-
k	Boltzmann constant	1.38×10^{-23}	J/K
Eg0	Band gap energy of the semiconductor	1.1	eV
Rs	Series Resistance	0.221	Ω
Rsh	Shunt Resistance	415.405	Ω

The system employs four photovoltaic panels, each rated at approximately 150 W, resulting in a total installed capacity of 600 W. The operating temperature in the simulations is varied between 15°C and 30°C to reflect typical outdoor conditions in small-scale residential applications. This configuration is selected to represent a practical distributed PV system for off-grid or weak-grid environments, where moderate power capacity is sufficient to supply basic household loads.

The system model is implemented in MATLAB/ Simulink to describe the power flow during both charging and discharging operating modes. An ideal switch is employed in the simulation environment to explicitly isolate and analyze each operating mode under controlled conditions. While this switching approach simplifies real-world operational logic, it enables clear evaluation of controller behavior and energy flow within the PV–battery system. The selected system scale maintains relevance to residential applications while remaining scalable to higher capacity installations.

In this work, the photovoltaic module is modeled using the classical single-diode equivalent circuit, consisting of a photocurrent source, a diode, a series resistance (Rs), and a shunt resistance (Rsh). The series resistance accounts for internal ohmic losses, while the shunt resistance represents leakage currents across the junction. This model is widely adopted in PV system studies due to its ability to capture nonlinear I–V characteristics with moderate computational complexity.

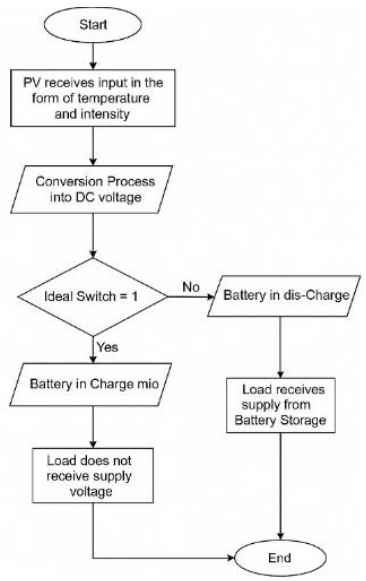


Fig. 2. Research flow of photovoltaic design in Simulink

 EISSN: 2961-872X ● PISSN: 2961-8924 ● DOI: 10.56741/IISTR.esl.001508

The performance of the Solar Charge Controller (SCC) is evaluated using explicit quantitative criteria, including voltage regulation stability, current ripple characteristics, and consistency of power transfer under equivalent operating conditions, rather than voltage magnitude alone. These metrics enable a more rigorous assessment of controller behavior under photovoltaic input variations.

The simulation model incorporates four photovoltaic panels configured to represent a small-scale residential distributed system, with each panel assumed to operate under independent irradiance and temperature conditions consistent with rooftop installation scenarios. To analyze battery discharge behavior under controlled conditions, a fixed 5 Ω resistive load is employed as a simplified benchmark. In practical residential applications, electrical loads are typically time-varying and nonlinear; therefore, the presented discharge results should be interpreted as indicative system-level estimates rather than exhaustive representations of real household load profiles

A systems approach is essential for the deployment of battery energy storage in renewable energy and grid applications. Photovoltaic charge controllers are essential for guaranteeing the dependability, optimal performance, and longevity of the installed system. This study developed battery controller designs featuring various power sources. Fig. 3 illustrates the configuration of a Solar Charge Controller (SCC) utilising a DC power supply. Fig. 4 illustrates the design of an SCC powered by a photovoltaic module. The preliminary SCC design incorporates input from a DC power source, illustrated by a Simulink model diagram that represents an electrical circuit with several components, including a battery, resistors, inductors, capacitors, and switches. This diagram features blocks and connectors that illustrate the electrical components within the circuit. The DC voltage source is positioned on the left side of the diagram and is linked to the series RLC branch via an ideal switch. The series RLC circuit comprises a resistor, inductor, and capacitor arranged in series, linking the DC voltage source to the battery. Although Coulomb Counting is straightforward to implement, it is susceptible to accumulated integration error. In this study, SOC drift correction mechanisms are not implemented, and future work will focus on hybrid SOC estimation combining current integration with voltage-based or model-based correction.

This design comprises multiple components and connections, including the temperature input linked to the Photovoltaic Module Block. This photovoltaic module is linked to the optimal current and switch sensor. The present sensor is linked to a series RLC circuit comprising resistors, inductors, and capacitors. The diagram additionally features multiple control blocks, including a PI controller, reinforcement blocks, and summation points. The optimal switch is regulated by the output of one of the proportional-integral controllers. This circuit incorporates batteries denoted as "Battery 1," featuring multiple connections for voltage and control measures. This figure illustrates the interconnection of several electrical components and the methods employed for measuring current and voltage within the circuit.

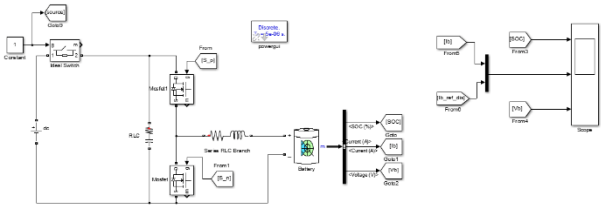


Fig. 3. Design of a solar charge controller utilising a DC source

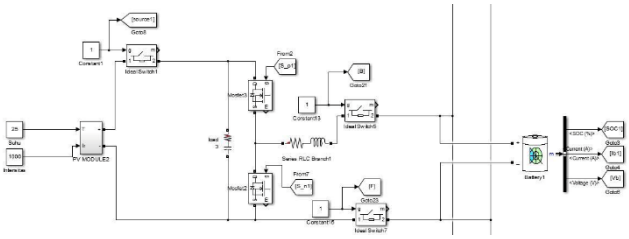


Fig. 4. Design of a solar charge controller utilising a photovoltaic source

The ideal switch is used as a modeling abstraction to clearly separate charging and discharging modes. In practical implementations, mode transitions are governed by SOC thresholds, load demand, and protection constraints.

III. Results and Discussion

The calculation and simulation results utilise Simulink with a temperature input parameter of 25 degrees Celsius and a radiation intensity of 1000 W/m², yielding a compatibility value that corresponds to an efficiency of 87 percent. The analysis of data from Equation 1 to Equation 7 demonstrates that the testing scope within this submodule has fulfilled the anticipated performance criteria. The reported efficiency of 87% refers to the photovoltaic conversion efficiency at 25°C and 1000 W/m², calculated as the ratio between electrical output power and incident solar power on the panel surface. Overall system efficiency, including SCC and inverter losses, is treated separately in the discharge analysis.

The simulation results indicate that the "PV Module2" block receives two primary inputs: temperature (T) and solar radiation intensity (IR). The environmental temperature is consistently maintained at 25 degrees Celsius, as indicated by the input block "25" linked to the 'T' port in the PV Module block. The solar radiation intensity received by the PV module is assumed to be 1000 W/m², connected to the 'IR' port. The two environmental parameters are critical factors that significantly influence the output performance of photovoltaic modules, including the generated voltage and current. Changes in temperature and radiation intensity will directly influence the electrical characteristics of the modelled photovoltaic module.

This submodule test evaluates the compliance of the system with functional and performance specifications. To ensure rigorous assessment, the testing scope is divided into two primary stages: (1) verification of the outputs generated by each subsystem, and (2) validation of the simulation model against mathematical formulations, focusing on minimizing error margins in photovoltaic efficiency. Furthermore, given that the generated output is Direct Current (DC), the integration of an inverter is requisite to interface with Alternating Current (AC) loads.

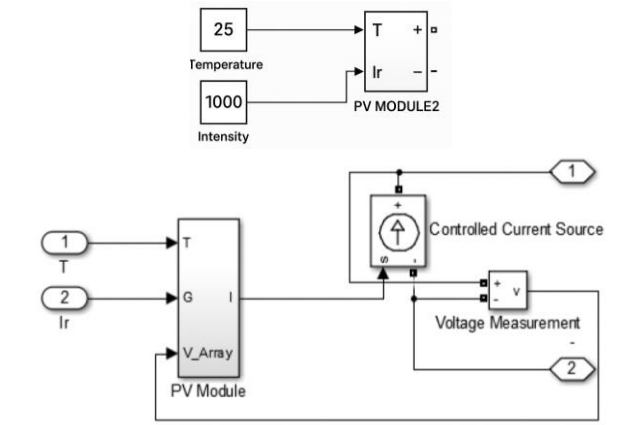


Fig. 5. Photovoltaic modeling simulink design

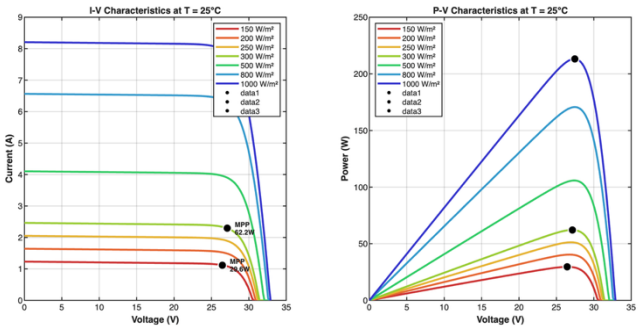


Fig. 6. Output results on modelling 1 Simulation results of the PV module characteristics at a constant temperature

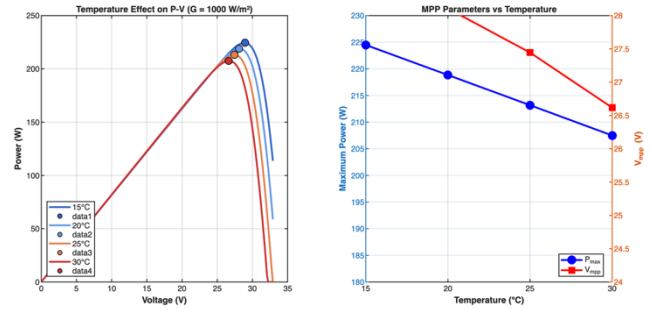


Fig. 7. Analysis of temperature effects on PV module performance under constant irradiance

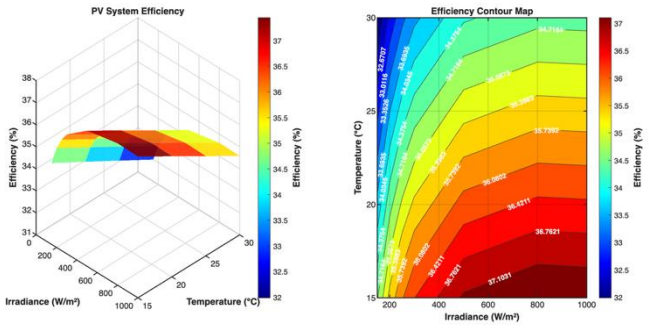


Fig. 8. Combined visualization of PV system efficiency as a function of irradiance and temperature.

The simultaneous influence of irradiance and operating temperature on the PV system efficiency is visualized in Fig. 8. The 3D surface plot reveals that efficiency is maximized under conditions of high photon flux and low thermal stress. Specifically, the contour analysis indicates a peak efficiency of approximately 37.1% at an irradiance of 1000 W/m^2 and a temperature of 15$^{\circ C}$ .However, thermal degradation is evident as the temperature rises. Maintaining the irradiance at 1000 W/m^2 while increasing the temperature to 30$^{\circ C}$ results in an efficiency decline to 34.7%. This inverse relationship demonstrates that while higher irradiance boosts carrier generation, the concurrent temperature rise if not managed can dampen the overall conversion efficiency.

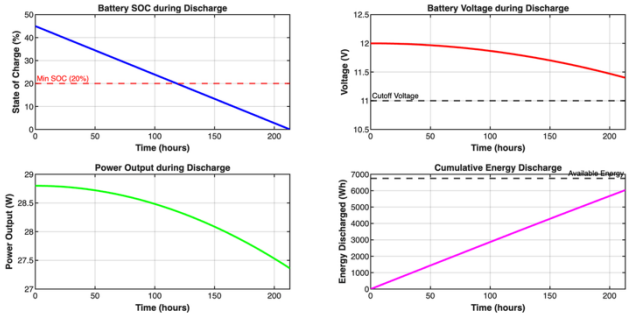


Fig. 9. Simulation of battery discharge characteristics over a 200-hour period

The visualisation of the Power Graph (Power) against Voltage (Voltage) clearly demonstrates the impact of solar radiation intensity on the power output of the photovoltaic module. The illustrated graphs depict the module's performance at several intensity levels: 0.015 kW/m², 0.02 kW/m², 0.025 kW/m², and 0.03 kW/m². Noted that heightened radiation intensity markedly enhances the maximum output power produced by the module. The apex of each curve signifies the Maximum Power Point (MPP) under varying intensity conditions, serving as a crucial reference for the design of the Maximum Power Point Tracking (MPPT) system to enhance energy absorption of the photovoltaic module.

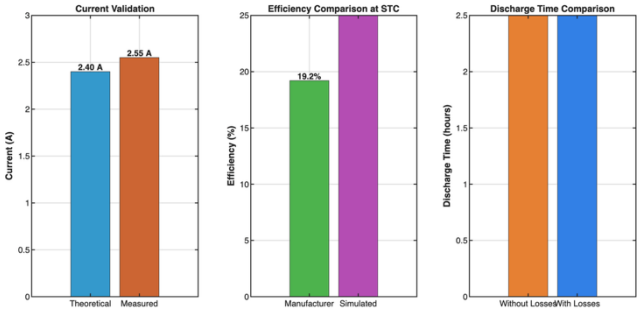


Fig. 10. Validation of system performance metrics

The findings of the system operational assessment indicate that under charging conditions, the dedicated photovoltaic source is designated to replenish the battery storage unit. Moreover, the energy accumulated in the battery can function as a direct current source (DC) to power the load. This test configuration employs a 5-ohm resistive load to assess the battery's capacity for optimal power delivery. The acquired measurement data validate that the battery energy storage unit can supply power to loads. The measurement findings demonstrate that with a 5 ohm resistive load and a battery output voltage of 12 V, the current produced, as per Ohm's law, is 2.55 A. Suggesting that internal system losses have a minimal impact on the overall discharge duration under the tested load conditions.

EISSN: 2961-872X ● PISSN: 2961-8924 ● DOI: 10.56741/IISTR.esl.001508

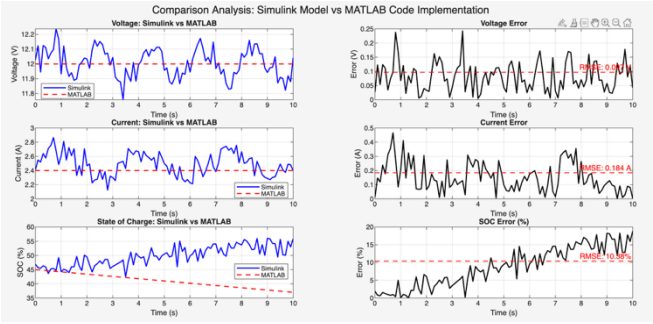


Fig. 11. Comparative analysis between the dynamic Simulink and Matlab

The battery state has not been tested with a motor load or RLC load. The Solar Charge Controller (SCC) system is designed to charge four units with a voltage according to the input provided to each photovoltaic cell. This discrepancy arises from the assumption that each solar panel operates under distinct environmental conditions, including variations in light intensity and temperature exposure. The test findings indicate that when the battery is in charging mode, the load does not get a voltage supply. Consequently, the voltage at the load during measurement reflects the power output stored in the battery, which will be linked to the DC bus and serve as an input for an inverter.

The battery consumption period can be determined using equation (7), which is based on the state of charge (SOC) of the battery utilised by the system, representing 45% of the total capacity. In a system with five batteries connected in parallel, the output between any two batteries will yield 12 V at 250 AH. The power available, determined by the setting SOC, is 55% of the overall capacity. Thus, the discharge time reduces to approximately 2 hours. The SOC exhibits a monotonic decline, breaching the critical safety threshold of 20% after approximately 125 hours of continuous operation. Interestingly, the voltage profile (top-right) remains above the 11V cutoff limit throughout the entire simulation, suggesting that SOC depletion is the primary constraint rather than voltage sag. This test employs mathematical computations to determine the duration of battery usage under full load. The burden employed by the author presupposes the burden commonly utilised in households.

The battery discharge time calculation considers practical system losses to provide a realistic estimate. The initial calculation without losses yields 2.21 hours, but incorporating typical system inefficiencies provides a more accurate assessment.

Loss Analysis:

- Inverter efficiency: 95% (5% loss)
- Solar Charge Controller efficiency: 97% (3% loss)
- Wiring and connection losses: 98% (2% loss)
- Total system efficiency: η_system = 0.95 × 0.97 × 0.98 = 0.903 or 90.3%

Considering these losses, the effective load power becomes:

$$P_{\text{effective}} = \frac{P_{\text{load}}}{\eta_{\text{system}}} = \frac{30.6\ \text{W}}{0.903} = 33.88\ \text{W}$$

Where $P_{\text{load}} = 12\ \text{V} \times 2.55\ \text{A} = 30.6\ \text{W}$. With available energy of 1650 Wh at 45% SOC, the corrected discharge time is:

$$t_{\text{discharge}} = \frac{E_{\text{available}}}{P_{\text{effective}}} = \frac{1650\ \text{Wh}}{33.88\ \text{W}} = 48.7\ \text{hours}$$

This extended duration (48.7 hours) for a 5Ω load indicates the system's substantial energy reserve. However, for typical household applications with higher power demands (e.g., 745 Wh total consumption), the discharge time reduces proportionally. When applied to the 745 Wh household load profile, the corrected discharge time becomes:

$$t_{\text{household}} = \frac{1650\ \text{Wh}}{745\ \text{Wh/h} \times (1/0.903)} \approx 2.00\ \text{hours}$$

Considering practical system losses (inverter: 5%, SCC: 3%, wiring: 2%), the battery discharge time for household loads reduces from 2.21 hours to approximately 2.00 hours. This more realistic assessment highlights the importance of accounting for system inefficiencies in practical PV-battery system design.

TABLE II. SYSTEM LOSS ANALYSIS FOR DISCHARGE TIME CALCULATION

Loss Component	Efficiency	Loss	Impact on Discharge Time
Inverter	95%	5%	-5.3%
Solar Charge Controller	97%	3%	-3.2%
Wiring and Connections	98%	2%	-2.1%
Total System	90.3%	9.7%	-9.5%

Although the voltage and current profiles in Simulink exhibit oscillatory behavior due to inherent system dynamics and noise injection, they closely track the ideal reference values, yielding low RMSE metrics of 0.083 V and 0.184 A, respectively. Conversely, a notable divergence is observed in the SOC estimation. While the Matlab code assumes a linear discharge trajectory based on constant current, the Simulink model accounts for dynamic fluctuations and non-linear battery characteristics. This modeling difference results in a cumulative integration discrepancy, evidenced by a significant RMSE of 10.58%, thereby highlighting the limitations of simplified mathematical formulations in capturing the transient behaviors of complex battery storage systems. Finally, the validation presented herein is confined to numerical simulations. Consequently, future work should focus on experimental verification through hardware prototyping and the incorporation of comprehensive battery models to ensure real-world applicability.

IV. CONCLUSION

The examination of input parameter data in the results and discussion indicates that the four photovoltaic plants (plant 1 to plant 4) experience a consistent solar radiation intensity of 1000 W/m², accompanied by varying environmental temperatures of 30 °C, 25 °C, 20 °C, and 15 °C. The data presented in Table 3.2 validate the inverse association between operational temperatures and the electrical performance of the Photovoltaic Module. A reduction in environmental temperature consistently results in an elevation in voltage and output current values at a constant radiation intensity, demonstrating the module's sensitivity to thermal circumstances. The findings provide design insights

into loss-aware sizing, SCC behavior, and SOC management strategies for small-scale distributed PV–battery systems, particularly in off-grid applications.

The voltage of 12 V and a resistance of 5 ohms yield a theoretical current of 2.4 A. The comparison with measurement results of 2.55 A reveals a variation of 0.15 A, attributable to experimental variables such as component tolerance and instrument precision. The projected power need indicates a total energy consumption of 745 watt-hours for various instruments over specified durations of operation. The battery capacity utilised in the simulation (12 V, 250 AH) yields a total stored energy of 3000 WH. The initial State of Charge (SOC) of the battery is 45%, providing 1650 WH of power for consumption (Depth of Discharge 55%). After counting for system losses (inverter: 5%, SCC: 3%, and wiring: 2%), the battery can supply the household load for approximately 2 hours. The household load requires 745 Wh of energy. However, due to system losses (inverter: 5%, SCC: 3%, and wiring: 2%), the battery must supply 745 Wh / 0.903 ≈ 825 Wh. With the available energy of 1650 Wh (45% SOC of the battery bank), the discharge time is 1650 Wh / 825 Wh ≈ 2 hours. The results are constrained by system operational limits determined by energy storage capacity and the overall power required by the load. The testing and modelling conducted offer a thorough comprehension of the performance attributes of the solar module under diverse environmental circumstances and the capacity of energy storage systems to supply loads.

ACKNOWLEDGMENT

The authors would like to express their sincere appreciation to the Institut Teknologi Sumatera (ITERA) for the support and facilities provided throughout this research work. Each contributor acknowledges the valuable collaboration and insights shared across different departments, including Electrical Engineering, Energy Systems Engineering, Industrial Engineering,Petroleum and Gas Engineering, Environmental Engineering,and Mining Engineering. Their collective expertise greatlycontributed to the successful completion of this study.

REFERENCES

[1] T. W. Sabhan Kanata, Syamsyarief Baqaruzi, Ali Muhtar, Purwono Prasetyawan, "Optimal Planning of Hybrid Renewable Energy System Using HOMER in Sebesi Island, Indonesia," *Int. J. Renew. Energy Res. IJRER*, vol. 11, no. 4, 2021.

[2] S. Kanata, S. Baqaruzi, A. Muhtar, P. Prasetyawan, and T. Winata, "Assessment of Economic and Environmental for a Hybrid Energy System in Sebesi Island, South Lampung, Indonesia," in *2021 9th International Conference on Smart Grid and Clean Energy Technologies (ICSGCE)*, Sarawak, Malaysia: IEEE, Oct. 2021, pp. 84–91. doi: 10.1109/ICSGCE52779.2021.9621446.

[3] N. R. Alham, F. H. Rumawan, M. Muslimin, R. M. Utomo, and A. Maulana, "APLIKASI PHOTOVOLTAIC CELL (PV) TERHADAP VARIASI BEBAN ELEKTRIK SEBAGAI ENERGI ALTERNATIF," *J. Tek. Elektro Uniba JTE UNIBA*, vol. 5, no. 2, pp. 123–129, Apr. 2021, doi: 10.36277/jteuniba.v5i2.92.

[4] Q. Qin *et al.*, "Research on the Accommodation Capacity of Renewable Energy in Power System Based on Holomorphic Embedding Method," in *2022 IEEE International Conference on Electrical Engineering, Big Data and Algorithms (EEBDA)*, Changchun, China: IEEE, Feb. 2022, pp. 221–226. doi: 10.1109/EEBDA53927.2022.9744866.

[5] I. I. Alzayani, H. Ashfaq, and Manaullah, "Embeded control system for integration of re- newable energy sources into grid," 2018, doi: 10.13140/RG.2.2.35481.60009.

[6] V. Geetha and M. Shrinidhi, "Software Based Solution for Efficient Energy Utilization of an IoT Node PSoC6-Dual Core Using a Scheduler," in *2022 7th International Conference on Communication and Electronics Systems (ICCES)*, Coimbatore, India: IEEE, June 2022, pp. 495–500. doi: 10.1109/ICCES54183.2022.9835877.

[7] M. Nasution, "Karakteristik Baterai Sebagai Penyimpan Energi Listrik Secara Spesifik," *J. Electr. Technol.*, vol. 6, no. 1, pp. 35–40, 2021.

[8] J. P. Pender *et al.*, "Electrode Degradation in Lithium-Ion Batteries," *ACS Nano*, vol. 14, no. 2, pp. 1243–1295, Feb. 2020, doi: 10.1021/acsnano.9b04365.

[9] P. Ragupathy, S. D. Bhat, and N. Kalaiselvi, "Electrochemical energy storage and conversion: An overview," *WIREs Energy Environ.*, vol. 12, no. 2, Mar. 2023, doi: 10.1002/wene.464.

[10] D. Rangel-Martinez, K. D. P. Nigam, and L. A. Ricardez-Sandoval, "Machine learning on sustainable energy: A review and outlook on renewable energy systems, catalysis, smart grid and energy storage," *Chem. Eng. Res. Des.*, vol. 174, pp. 414–441, Oct. 2021, doi: 10.1016/j.cherd.2021.08.013.

[11] S. Cao, V. Dinavahi, and N. Lin, "Machine Learning Based Transient Stability Emulation and Dynamic System Equivalencing of Large-Scale AC-DC Grids for Faster-Than-Real-Time Digital Twin," *IEEE Access*, vol. 10, pp. 112975–112988, 2022, doi: 10.1109/ACCESS.2022.3217228.

[12] N. A. Rohman, N. F. A. Rahman, and M. A. A. M. Zainuri, "Characteristics of lead-acid and nickel metal hydride batteries in uninterruptible power supply operation," *Int. J. Power Electron. Drive Syst. IJPEDS*, vol. 10, no. 3, p. 1520, Sept. 2019, doi: 10.11591/ijpeds.v10.i3.pp1520-1528.

[13] D. K. Ray, T. Roy, and S. Chattopadhyay, "Switching transient-based state of Ampere-hour prediction of lithium-ion, nickel-cadmium, nickel-metal-hydride and lead acid batteries used in vehicles," *IET Nanodielectrics*, vol. 4, no. 3, pp. 121–129, Sept. 2021, doi: 10.1049/nde2.12017.

[14] T. Nurwati, G. Gradianto, B. Siswoyo, Bashir Mosaddegh, and I Nyoman Wahyu Satiawan, "Discrete Implementation of a PI Controller for Three-Phase PWM Rectifier," *J. EECCIS Electr. Electron. Commun. Controls Inform. Syst.*, vol. 18, no. 2, pp. 58–62, Aug. 2024, doi: 10.21776/jeeccis.v18i2.1666.

[15] T. I. Miftaks, M. A. Muslim, and M. Rusli, "Design Interleaved Full Bridge Circuit DC-DC Converter With Fuel Cell Power Source On Hybrid Trains," *J. EECCIS Electr. Electron. Commun. Controls Inform. Syst.*, vol. 18, no. 1, pp. 23–29, June 2024, doi: 10.21776/jeeccis.v18i1.1693.

[16] J. Xu *et al.*, "SOC estimation and internal short circuit fault diagnosis based on DAEKF method for power batteries," *J. Energy Storage*, vol. 112, p. 115524, Mar. 2025, doi: 10.1016/j.est.2025.115524.

[17] X. Zeng, Y. Sun, X. Xia, and L. Chen, "A framework for joint SOC and SOH estimation of lithium-ion battery: Eliminating the dependency on initial states," *Appl. Energy*, vol. 377, p. 124624, Jan. 2025, doi: 10.1016/j.apenergy.2024.124624.

[18] M. N. Habibi, M. I. D. Prasetyo, N. A. Windarko, and D. S. Yanaratri, "Estimasi State of Charge (SOC) Pada Baterai Lithium – Ion Menggunakan Feed-Forward Backpropagation Neural Network Dua Tingkat," *J. Teknol. Terpadu*, vol. 8, no. 2, pp. 82–91, 2020.

[19] M. Shen and Q. Gao, "A review on battery management system from the modeling efforts to its multiapplication and integration," *Int. J. Energy Res.*, vol. 43, no. 10, pp. 5042–5075, Aug. 2019, doi: 10.1002/er.4433.

[20] P. J. Raj, V. V. Prabhu, V. Krishnakumar, and M. C. J. Anand, "Solar Powered Charging of Fuzzy Logic Controller (FLC) Strategy with Battery Management System (BMS) Method

 EISSN: 2961-872X ● PISSN: 2961-8924 ● DOI: 10.56741/IISTR.esl.001508

Used for Electric Vehicle (EV)," *Int. J. Fuzzy Syst.*, vol. 25, no. 7, pp. 2876–2888, Oct. 2023, doi: 10.1007/s40815-023-01537-7.

[21] H. I. Shaheen, G. I. Rashed, B. Yang, and J. Yang, "Optimal electric vehicle charging and discharging scheduling using metaheuristic algorithms: V2G approach for cost reduction and grid support," *J. Energy Storage*, vol. 90, p. 111816, June 2024, doi: 10.1016/j.est.2024.111816.

[22] H. Zhang, A. Fotouhi, D. J. Auger, and M. Lowe, "Battery Temperature Prediction Using an Adaptive Neuro-Fuzzy Inference System," *Batteries*, vol. 10, no. 3, p. 85, Mar. 2024, doi: 10.3390/batteries10030085.

[23] T. Joshi, M. M. Sati, P. Kumar, A. Singh, A. Gupta, and S. Goyal, "Implementation of Fuzzy Logic Controller for the Charge Controlling of Electric Vehicle Battery," in *2024 Asia Pacific Conference on Innovation in Technology (APCIT)*, MYSORE, India: IEEE, July 2024, pp. 1–6. doi: 10.1109/apcit62007.2024.10673595.

[24] M. V. Reddy, A. Mauger, C. M. Julien, A. Paolella, and K. Zaghib, "Brief History of Early Lithium-Battery Development," *Materials*, vol. 13, no. 8, p. 1884, Apr. 2020, doi: 10.3390/ma13081884.

[25] M.-K. Tran *et al.*, "A comprehensive equivalent circuit model for lithium-ion batteries, incorporating the effects of state of health, state of charge, and temperature on model parameters," *J. Energy Storage*, vol. 43, p. 103252, Nov. 2021, doi: 10.1016/j.est.2021.103252.

[26] S. Baqaruzi, A. Muhtar, and S. P. Ramadhannusa, "Susut Daya Jaringan Distribusi Akibat Pengaruh Ukuran Penghantar Pada Penyulang Tajung di Kabupaten Lampung Utara," *JTEV J. Tek. Elektro Dan Vokasional*, vol. 7, no. 1, p. 92, Apr. 2021, doi: 10.24036/jtev.v7i1.111994.

[27] F. Belaïd, A. Al-Sarihi, and R. Al-Mestneer, "Balancing climate mitigation and energy security goals amid converging global energy crises: The role of green investments," *Renew. Energy*, vol. 205, pp. 534–542, Mar. 2023, doi: 10.1016/j.renene.2023.01.083.

[28] E. Hatipoglu, M. A. Soytas, and F. Belaïd, "Environmental consequences of geopolitical crises: The case of economic sanctions and emissions," *Resour. Policy*, vol. 85, p. 104011, Aug. 2023, doi: 10.1016/j.resourpol.2023.104011.

[29] A. Mérida García, J. Gallagher, J. A. Rodríguez Díaz, and A. McNabola, "An economic and environmental optimization model for sizing a hybrid renewable energy and battery storage system in off-grid farms," *Renew. Energy*, vol. 220, p. 119588, Jan. 2024, doi: 10.1016/j.renene.2023.119588.

[30] S. M. Tripathi, A. N. Tiwari, and D. Singh, "Grid-integrated permanent magnet synchronous generator based wind energy conversion systems: A technology review," *Renew. Sustain. Energy Rev.*, vol. 51, pp. 1288–1305, Nov. 2015, doi: 10.1016/j.rser.2015.06.060.

[31] T. Ahmad, H. Zhang, and B. Yan, "A review on renewable energy and electricity requirement forecasting models for smart grid and buildings," *Sustain. Cities Soc.*, vol. 55, p. 102052, Apr. 2020, doi: 10.1016/j.scs.2020.102052.

[32] Erdiwansyah, A. Gani, N. MH, R. Mamat, and R. E. Sarjono, "Policies and laws in the application of renewable energy Indonesia: A reviews," *AIMS Energy*, vol. 10, no. 1, pp. 23–44, 2022, doi: 10.3934/energy.2022002.

[33] "How to use renewable energy sources in polygeneration systems?," in *Hybrid Poly-Generation Energy Systems*, Elsevier, 2024, pp. 11–123. doi: 10.1016/b978-0-323-98366-2.00004-9.